

Four New Eclipsing Binary Systems in the TESS field: CD-34 13220, HD 295082, TYC 6484-426-1 and TYC 6527-2310-1

Burak Ulaş^{1,2}

¹ Department of Space Sciences and Technologies, Faculty of Arts and Sciences, Çanakkale Onsekiz Mart University, Terzioğlu Campus, TR 17100, Çanakkale, Turkey; *burak.ulas@comu.edu.tr*

² Astrophysics Research Centre and Observatory, Çanakkale Onsekiz Mart University, Terzioğlu Campus, TR 17100, Çanakkale, Turkey

Received 20XX Month Day; accepted 20XX Month Day

Abstract We present the first evidence for the binarity of four targets in the TESS field. The temperatures are estimated by SED analysis and the orbital periods are determined. The TESS light curves of the systems are analysed and the orbital and the absolute parameters are derived. The targets are also compared to well-studied binary systems with the same morphological type and their evolutionary states are discussed. Our results indicate that the stars belong to the class of eclipsing detached binary systems.

Key words: binaries: eclipsing — stars: fundamental parameters — stars: individual: CD-34 13220, HD 295082, TYC 6484-426-1, TYC 6527-2310-1

1 INTRODUCTION

Binary stars are significant stellar objects in the sense of allowing the researchers to determine the physical parameters of the components precisely and investigate the stellar evolution of the stars in various circumstances. Ever since Giovanni B. Riccioli's observation of Mizar in the 17th century and Christian Mayer's first catalog of double stars in 1781, astronomers forge away in understanding the light variation and physical properties of these types of systems. The number of newly discovered binary star systems were increased at the beginning of the 1900s, the years when the astronomers were keen on finding new systems, as mentioned in Niemela (2001). At present time, a recently updated version of Binary Star Database (Kovaleva et al. 2015) consists of about 120000 stellar systems. A growing number of space-based observations also made a major contribution to the discovery and investigation of the properties of the component stars in detail, thanks to their precise data. Eclipsing binaries, a subclass of binary star systems, are also important tools in astrophysics in understanding the structure and characteristics of the stars. The analyses of the

like mass, radius, luminosity, and temperature but also structural phenomena just as apsidal motion and atmospheric parameters such as limb darkening, gravity darkening as remarked by Guinan (1993).

Our information on several stellar phenomena, including binarity, was increased by recent space-based missions like *Kepler* Borucki et al. (2010) and Transiting Exoplanet Survey Satellite (TESS, Ricker et al. 2015). For instance, Kepler Eclipsing Binary Catalog (Kirk et al. 2016) consists of light curves and the related parameters of 2878 systems. TESS, on the other hand, is very opportune in studying low amplitude variations such as the light curves of pulsating stars in binary systems. The mission focused on the identification of transiting planets around nearby stars by scanning the 85% of the sky in its first two years (Ricker et al. 2015). The several parameters of approximately 400000 selected stars are planned to be cataloged in TESS Input Catalog (TIC, Stassun et al. 2019). In addition to the above programs, ground-based surveys like The Large Sky Area Multi-Object Fiber Spectroscopic Telescope (LAMOST, Zhao et al. 2012) and The All Sky Automated Survey (ASAS, Pojmanski 2002) provided a great improvement in the discovery and the knowledge of the structure and the evolution of binary stars. For example, the atmospheric parameters of 2020 EA- and 9149 EW-type binary systems observed by LAMOST were cataloged, and their evolutionary states were discussed by Qian et al. (2018) and Qian et al. (2020). 256000 binary or variable star candidates were also detected by Qian et al. (2019) among 786400 stars falling into the field of LAMOST.

The targets investigated in this study are not classified as eclipsing binary systems in the literature so far. CD-34 13220 (TIC 277373390) can be found in several catalogs (Thome 1994; National Aeronautics and Space Administration 1993; Morrison et al. 2001; Cutri et al. 2003; Röser et al. 1994; Høg et al. 2000; Gaia Collaboration et al. 2018) which list the position and magnitude information of the stars substantially. Cruzalèbes et al. (2019) list HD 295082 (TIC 42828781) in their Mid-infrared Stellar Diameters and Fluxes Compilation Catalogue with the estimated distance and angular diameter values of 533.2 pc and 0.063 mas, respectively. The star also appears in The Henry Draper Extension Charts (Nesterov et al. 1995) in which the spectral class, position, and magnitude values are tabulated. TYC 6484-426-1 (TIC 31303242) is in the photometric empirical calibration research of Ruiz-Dern et al. (2018). They included the star to the list of targets with low extinction by giving $E(B - V)_{max} = 0.0083$. Cantat-Gaudin et al. (2018) remarked that TYC 6527-2310-1 (TIC 63192395) is not belonging to an open cluster in their study on astrometric parameters of 128 open clusters. The star was also listed among the solar-like oscillators in the TESS field by Schofield et al. (2019) which gives fundamental parameters combining the Gaia DR2 and Hipparcos data.

The lack of comprehensive studies in the literature motivated us to investigate the systems in detail. In the next section, we give the properties of the data and features of the TESS light curves. The details of the light curve analyses and the results proving our targets' binarity are explained in Sec 3. The last section deals with the discussion of the results, evolutionary status, and comparison of the systems to well-known

2 LIGHT CURVE DATA

The TESS light curves of the systems were acquired from the light curve files that were achieved through MAST (Mikulski Archive of Space Telescope Portal)¹. The files contain data that the photometric analysis and cotrending were applied (Tanenbaum & Jenkins 2018). The PDC_SAP (Pre-search Data Conditioning Simple Aperture Photometry) flux values (F_i) were extracted from the data files and converted to magnitudes (m_i) by using the equation $m_i = -2.5 \log F_i$. The TESS magnitudes (9.45^m , 9.74^m , 10.14^m , and 9.60^m for CD-34 13220, HD 295082, TYC 6484-426-1, and TYC 6527-2310-1, respectively) given by Stassun et al. (2019) were used during the derivation of the magnitudes. A linear trend as a function of time was also removed from the data of TYC 6484-426-1 and TYC 6527-2310-1. Fig. 1 shows the systems' light variations in one orbital period intervals. These curves represent the common eclipsing binary type variations.

The depth of the primary and secondary minimums are 0.49^m and 0.35^m for CD-34 13220, 0.63^m and 0.55^m for HD 295082, 0.50^m and 0.45^m for TYC 6484-426-1 and 0.44^m and 0.41^m for TYC 6527-2310-1. Primary minimum lasts 3.8^h , 9.8^h , 9.6^h , and 8.4^h for CD-34 13220, HD 295082, TYC 6484-426-1, and TYC 6527-2310-1, respectively, while the durations of the secondary minimums are 3.6^h , 9.1^h , 9.6^h , and 8.2^h . The data are from observation sector 13 for CD-34 13220, sector 6 for HD 295082, sector 5 and 6 for TYC 6484-426-1, and sector 6 and 7 for TYC 6527-2310-1. Furthermore, the lack of minima times in the literature directed us to calculate times of minimum lights for the systems using the method of Kwee & van Woerden (1956). Table 1 lists 92 calculated times of primary and secondary minimums. In the table, TYC 6484 and TYC 6527 refer to TYC 6484-426-1 and TYC 6527-2310-1, respectively.

The shape and the characteristics of the light curves verge upon the light variation of a common detached eclipsing binary system. Therefore, detached morphology must be considered during the analyses, as we introduce it in the next section.

3 ANALYSES OF THE LIGHT CURVES

One of the most critical parameters to achieve realistic results in the light curve analysis is the effective temperature of the primary component. Since there is very limited information on the systems in the literature, we estimated the temperatures of the primaries by constructing spectral energy distributions (SED) through Virtual Observatory SED Analyzer (VOSA, Bayo et al. 2008) for the available photometric data in the VizieR database (Ochsenbein et al. 2000). Parameter-grid search was used to fit the photometric data to achieve the optimized Kurucz atmosphere model (Kurucz 1979). The process was done for each system in the present study and the results were assumed to be the effective temperature of the primary components.

The absence of sufficient knowledge of the orbital properties of systems in the literature led us to determine orbital period values to be used in the light curve analyses. For doing this, we first employed Fourier analysis to the light curve data of each system using PERIOD04 software (Lenz & Breger 2005) and obtained a frequency value that corresponds to the orbital period. Alternatively, we averaged the differences between consecutive time of minimum lights of the same types to estimate a period value. From those two values, which constructs the better light curve was adopted as the orbital period for each system. Period

Table 1 Calculated times of minimum light for the systems

System	BJD-2457000	Type	System	BJD-2457000	Type	System	BJD-2457000	Type
CD-34 13220	1657.169086(5)	I	HD 295082	1677.021844(5)	I	TYC 6527	1476.51675(1)	I
	1656.585189(7)	II		1677.605866(7)	II		1483.57357(1)	I
	1658.336961(5)	I		1678.189751(5)	I		1479.96552(1)	II
	1657.753109(9)	II		1678.774260(9)	II		1487.02209(1)	II
	1659.504652(5)	I		1679.357437(5)	I		1468.81026(1)	I
	1658.920870(7)	II		1679.941601(7)	II		1470.34182(1)	II
	1660.671987(5)	I		1680.525091(5)	I		1471.87524(1)	I
	1660.088789(7)	II		1681.109487(7)	II		1473.40676(1)	II
	1661.840223(5)	I		1470.39149(1)	I		1474.94005(1)	I
	1661.256646(7)	II		1468.91985(1)	II		1476.47153(1)	II
	1663.008070(5)	I		1473.33431(1)	I		1481.06986(1)	I
	1662.424379(7)	II		1471.86274(1)	II		1479.53642(1)	II
	1664.175831(6)	I		1476.27736(1)	I		1484.13472(1)	I
	1663.592091(7)	II		1474.80601(1)	II		1482.60138(1)	II
	1664.760032(7)	II		1479.22043(1)	I		1487.19953(1)	I
	1666.511393(5)	I		1480.69188(1)	II		1485.66590(1)	II
	1665.927797(7)	II		1482.16348(1)	I		1493.32929(1)	I
	1668.847170(5)	I		1483.63491(1)	II		1491.79568(1)	II
	1669.431362(7)	II		1485.10649(1)	I		1496.39400(1)	I
	1670.014987(5)	I		1486.57796(1)	II		1494.86020(1)	II
1670.599053(7)	II	1488.04936(1)	I	1499.45889(1)	I			
1671.182855(5)	I	1489.52086(1)	II	1497.92537(2)	II			
1671.766854(7)	II	TYC 6484	1441.23240(2)	I	1502.52388(1)	I		
1672.350583(5)	I		1444.68152(1)	II	1500.99050(1)	II		
1672.934813(7)	II		1448.28973(1)	I	1505.58870(1)	I		
1673.518278(5)	I		1455.34646(1)	I	1507.11994(1)	II		
1674.102572(7)	II		1451.73825(1)	II	1508.65350(1)	I		
1674.686146(5)	I		1462.40318(1)	I	1510.18469(1)	II		
1675.270310(7)	II		1458.79505(1)	II	1511.71839(1)	I		
1675.854005(5)	I		1469.45999(1)	I	1513.24959(1)	II		
1676.438160(7)	II		1472.90868(1)	II				

analyses were also conducted to times of minimum in Table 1 by assuming a linear trend. Variation in time of minimum light (ΔT_0) and orbital period (ΔP) were calculated using the equation $O-C = \Delta T_0 + \Delta P \cdot E$, where E is the cycle number. Results are listed for each system in the last two lines of Table 2 and Fig. 4 and 5 are plotted by using the final period values.

The mass ratio is another significant parameter in the light curve analysis, just as temperature and orbital period mentioned in the previous paragraphs. The lack of any research related to the mass ratios of the systems in the literature pointed us to apply the q -search technique to the light curves in order to estimate mass ratio values. Although the shapes of the light curves and the orbital period values imply that the systems are detached binaries, we applied q -search to the systems' binned light curves covering 1500 data points in both detached and conventional semi-detached mode since there is no information about the

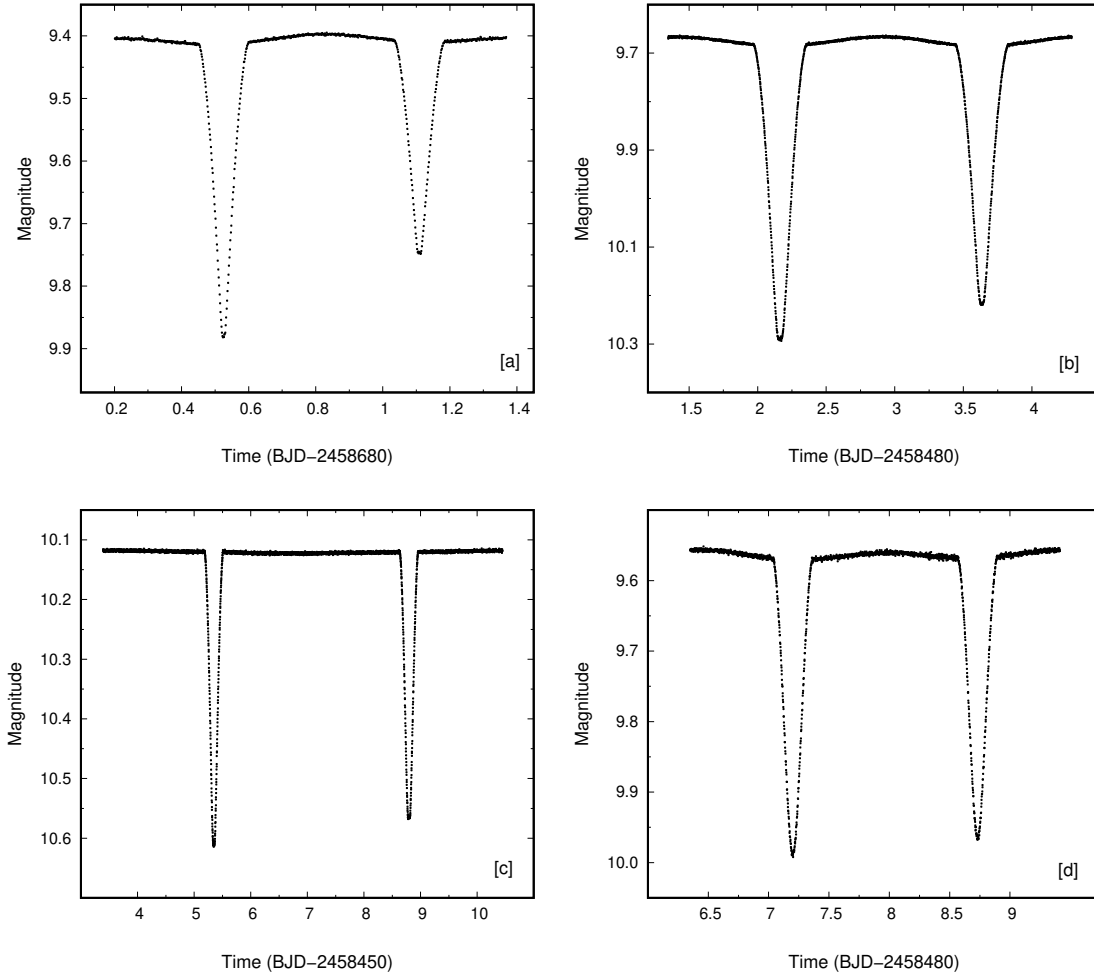


Fig. 1 One-period-long light curves of CD-34 13220 (a), HD 295082 (b), TYC 6484-426-1 (c), and TYC 6527-2310-1 (d). Magnitudes are calculated by using the TESS magnitudes given in Stassun et al. (2019).

residuals) of the solutions with two assumptions confirmed that the systems are detached binaries, as it can easily be hypothesized from the light curve shapes even at the first glance. The results are given in Fig. 2.

We analysed the TESS light curves using the `PHOEBE` (Prša & Zwitter 2005) which uses the Wilson-Devinney method (Wilson & Devinney 1971) to solve the light curve and obtain the stellar parameters from the input data. Following the results of the q -search, we applied analyses by assuming that the systems are detached binaries. The adjustable parameters are the inclination i , the temperature of the secondary component T_2 , mass ratio q , the surface potential values of both components Ω_1 and Ω_2 , and luminosity of the primary component L_1 during the solutions. The albedos ($A_1 = A_2 = 0.5$) are calculated from Ruciński (1969) and the gravity darkening coefficients ($g_1 = g_2 = 0.32$) for the systems was adopted from von Zeipel (1924) and Lucy (1967) by considering the granulation boundary for main sequence stars located at about F0 spectral type (Gray & Nagel 1989). Logarithmic limb darkening coefficients (x_1 and x_2) were adjusted from Claret (2017) based on the initial temperatures of the components and given in Table 2. In the table, the uncertainties in T_1 are listed as obtained in SED analyses, 2450000 is subtracted from the times of

2310-1, respectively. The fill-out factors for the components, f , were also calculated by using the relation $f = \frac{r}{r_L}$, where $r_L = \frac{0.49q^{\frac{2}{3}}}{0.6q^{\frac{2}{3}} + \ln(1+q^{\frac{1}{3}})}$, the volume radius of the Roche lobe, given by Eggleton (1983).

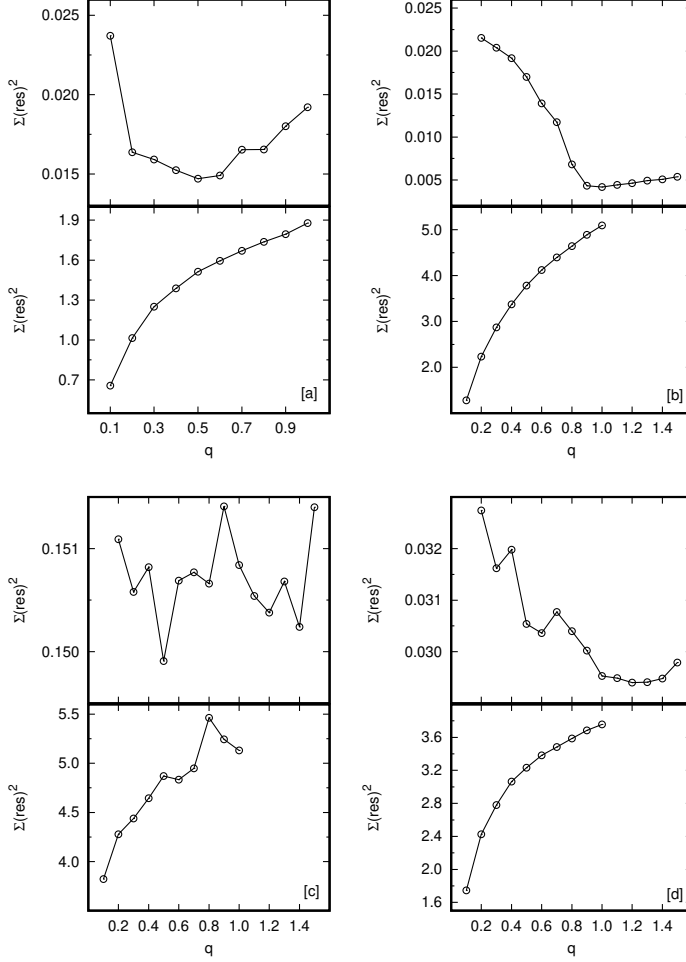


Fig. 2 Results of the q -searches for CD-34 13220 (a), HD 295082 (b), TYC 6484-426-1 (c), and TYC 6527-2310-1 (d). The upper and lower panels refer to the solutions in detached and semi-detached assumptions.

3.1 CD-34 13220

The temperature of the primary component was derived by SED analysis, as remarked in the previous section. The effective temperature interval was set 6000-6500 K during the SED analysis, comprising the temperatures, 6152 K of Gaia Collaboration et al. (2018) and 6345 K of Stassun et al. (2019). The $\log g$ interval was selected as 2.5-5.0 following TESS Input Catalog (TIC, Stassun et al. 2019). The extinction, $A_V=0.2246^m$, was calculated using the Galactic Dust Reddening and Extinction interface of NASA/IPAC Infrared Science Archive². The results of the SED analysis were $T_e=6250\pm 125$ and $\log g=4.50\pm 0.25$. Therefore, the initial effective temperature of the primary was taken as 6250 K during the light curve solution. Fig. 3 shows the model fit of the SED analysis.

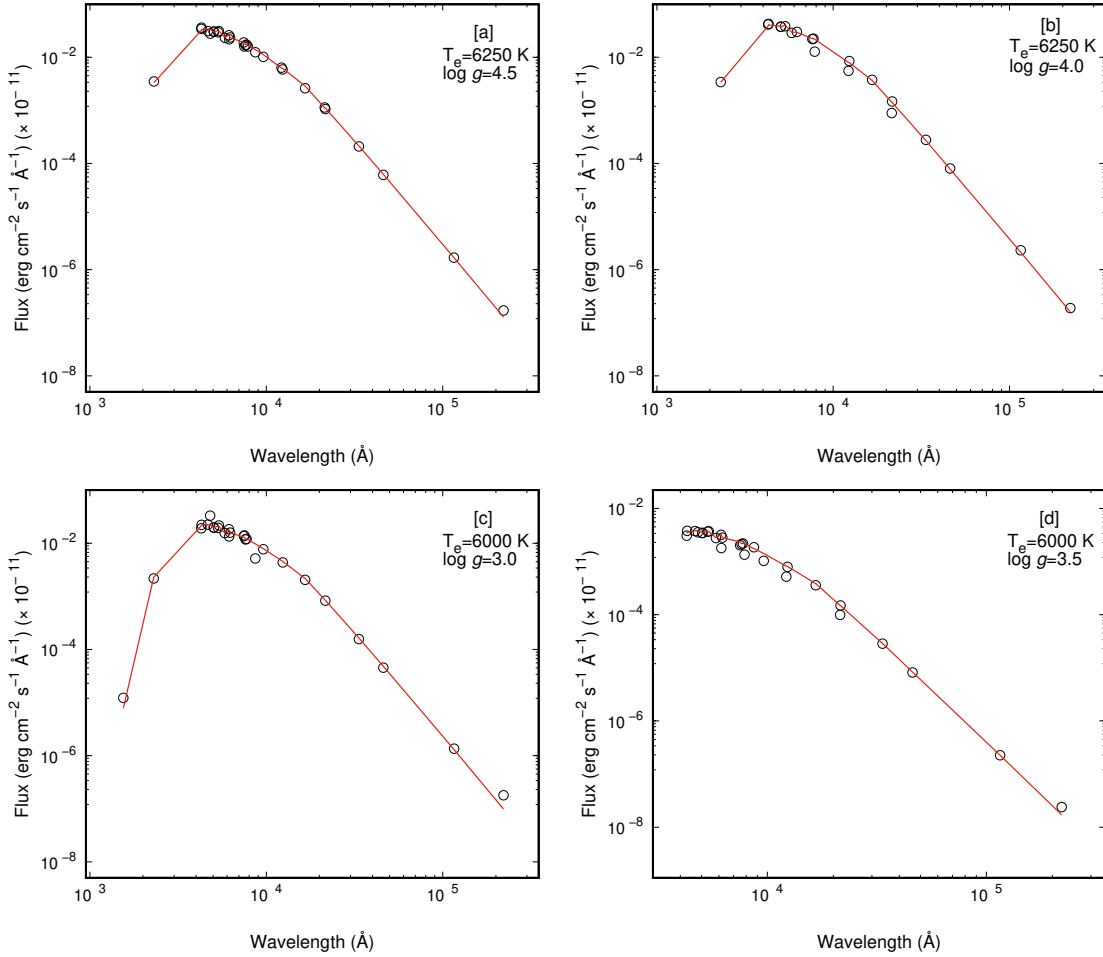


Fig. 3 Results of the SED analyses for CD-34 13220 (a), HD 295082 (b), TYC 6484-426-1 (c), and TYC 6527-2310-1 (d). Open circles indicate the photometric flux values from the VizieR database (Ochsenbein et al. 2000) and the solid (red in colored version) lines refer to the model fit. Final effective temperature and $\log g$ values are given on the upper right of each figure. Please note that the axes are on a logarithmic scale.

The light curve analysis was applied on 17766 data points in detached binary mode with the initial mass ratio value of 0.5 which was yielded by q -search. The orbital frequency was derived as $0.85551d^{-1}$ by using PERIOD04 which corresponds to 1.1694 days. However, a more appropriate value, 1.167802 days, was found by calculating the average of differences between consecutive times of minimum lights (see Sec. 3). Moreover, as magnitude difference between two maxima of the light curve exists, the best solution was achieved adopting a spotted area on the secondary component with the parameters of co-latitude $\beta=45^\circ$, longitude $\lambda=270^\circ$, spot radius $r=10^\circ$, and the temperature factor $T_f=0.9$. The observations and the synthetic light curve are shown together in Fig. 4. The resulting light parameters are listed in Table 2.

3.2 HD 295082

Our SED analysis resulted in temperature and surface gravity values of $T_e=6250\pm 125$ and $\log g=4.00\pm 0.25$. The initial interval of effective temperature was set 6000-7000 K during the analysis

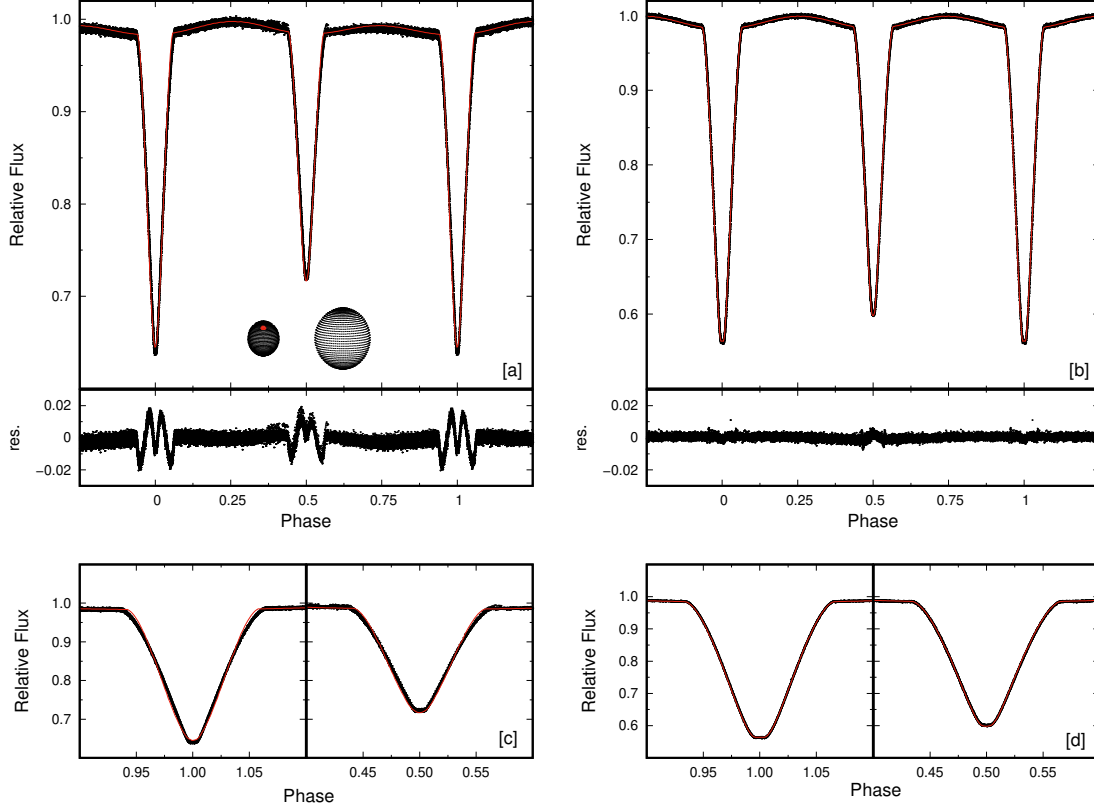


Fig. 4 Observational data with the synthetic light curves (red in colored version) of CD-34 13220 (a) and HD 295082 (b). The agreement of the fits are also shown at primary and secondary minimums for CD-34 13220 (c) and HD 295082 (d). The geometry of CD-34 13220 at phase 0.75 is also presented in (a) for the visibility of the spotted area (red) on the secondary component.

et al. (1995). The $\log g$ interval was 3.0-4.0 considering the value of 3.5 given by TIC (Stassun et al. 2019) and the visual extinction was derived as 1.0618^m . The fit of the SED analysis plotted with the photometric data in Fig. 3.

The light curve analysis was conducted with 14831 data points composing the light curve. During the analysis, the initial value of mass ratio was taken as 1.0, the result of our q -search. The orbital frequency was found to be $0.3352d^{-1}$ (2.9832 days) and 2.9430013 days by using two methods in Sec. 3 and set the latter one through the light curve solution process. The agreement between the theoretical light curve and observations is shown in Fig. 4. The final parameters found by the analysis are given in Table 2.

3.3 TYC 6484-426-1

The SED analysis ended up with the values of $T_e=6000\pm 125$ and $\log g=3.00\pm 0.25$ based on the initial interval of 6000-6250 K and 3.0-4.0 for the effective temperature and surface gravity, respectively, following the values given by Gaia Collaboration et al. (2018) and Stassun et al. (2019) (Fig. 3).

The analysis was applied to the light curve which consists of 31924 data points. The initial mass ratio was 0.5 and the calculated value of the orbital period is 7.056833 days. Differently from our other

Table 2 Results of the light curve analyses. r_1 and r_2 refer to the fractional radii. The standard deviations, 3σ for the last digits of light parameters are given in parentheses

Parameter	CD-34 13220	HD 295082	TYC 6484	TYC 6527
i ($^\circ$)	82.38(2)	87.78(1)	87.80(1)	84.59(1)
q	0.443(1)	1.001(1)	0.538(1)	1.195(2)
T_1 (K)	6250(125)	6250(125)	6000(125)	6000(125)
T_2 (K)	5904(17)	6055(10)	5970(24)	5936(20)
Ω_1	3.473(9)	6.622(2)	13.30(1)	8.299(6)
Ω_2	3.642(6)	5.459(3)	8.62(1)	6.850(9)
$\frac{L_1}{L_1+L_2}$	0.588(1)	0.4178(2)	0.541(1)	0.338(1)
r_1	0.199(3)	0.1785(7)	0.078(3)	0.141(2)
r_2	0.189(5)	0.226(1)	0.073(3)	0.202(2)
f_1	0.64(1)	0.471(2)	0.24(1)	0.357(5)
f_2	0.61(2)	0.596(3)	0.22(1)	0.512(5)
x_1, x_2	0.586, 0.601	0.583, 0.599	0.595, 0.611	0.597, 0.597
T_0 (BJD)	1657.169086(5)	1470.39149(1)	1441.23240(2)	1468.81026(1)
P (days)	1.167802(3)	2.9430013(9)	7.056833(1)	3.064855(2)

$e=0.0540(6)$. The synthetic light curve is plotted with the observational data in Fig. 5 and the results are tabulated in Table 2.

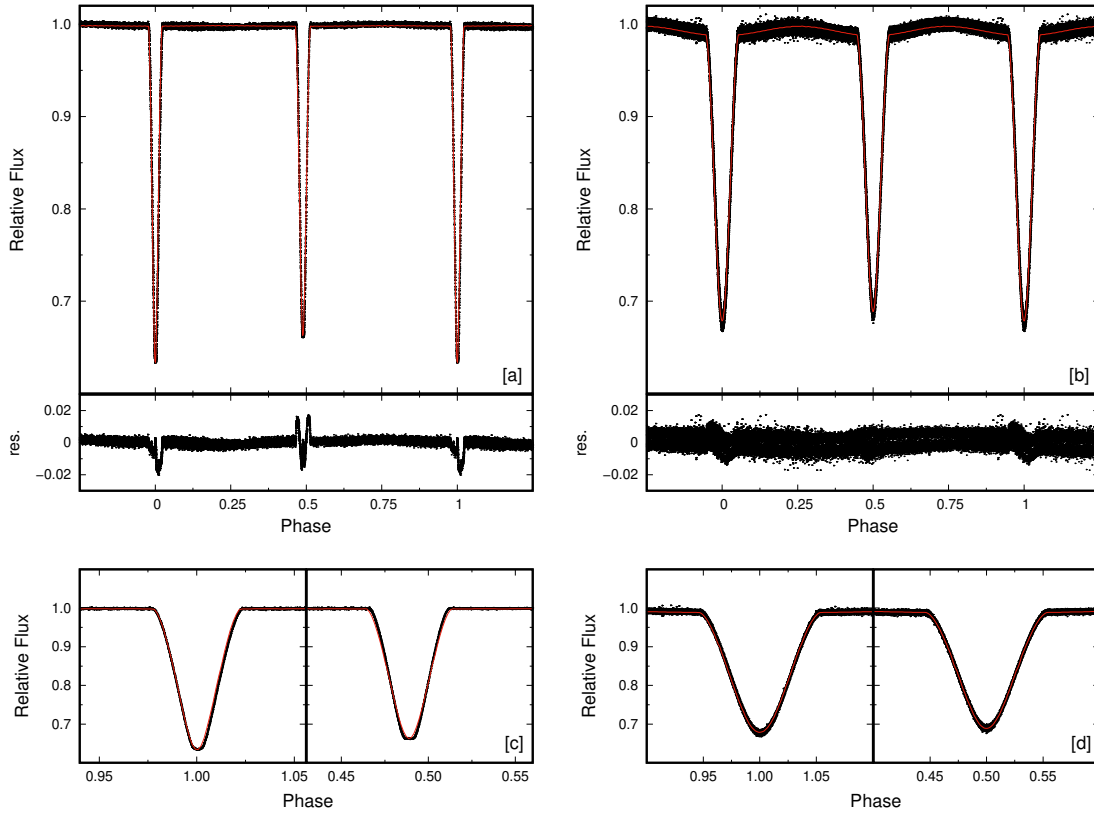


Fig. 5 Same as Fig. 4, but for TYC 6484-426-1 (a and c), and TYC 6527-2310-1 (b and d).

3.4 TYC 6527-2310-1

The temperature of the primary component was assumed to be 6000 ± 125 K and the $\log g$ is 3.50 ± 0.25 , the results of the SED model fit. The SED analysis was applied by using the initial parameters of the effective temperature between 5750 and 6000 K and gravity between 3.0 and 5.0 by following values of Gaia Collaboration et al. (2018), Schofield et al. (2019), Stassun et al. (2019). The result is plotted with photometric data in Fig. 3.

31191 data points were analysed during the light curve solution with the initial mass ratio value of 1.2 from the q -search. The orbital period was derived as 3.064855 days. Results show that the secondary component is more massive and luminous than the primary as shown in Table 2. Observational and synthetic light curves are plotted in Fig. 5.

We also investigated the solar-like oscillation candidacy of the star, as it was included in the asteroseismic target list of Schofield et al. (2019). Although the temperature of the target (6250 K) can be considered as close to solar temperature, the period analyses conducted with `PERIOD04` did not result in any frequency close to 3mHz, the frequency of the highest amplitude oscillation of Sun. Therefore, we do not confirm the probable oscillational behavior of the star based on our analysis.

4 CONCLUSION

We present the first results proving that the systems in question are detached binaries. The effective temperature and $\log g$ values were estimated for primaries by using model fits from the SED analyses. The orbital periods were determined by applying frequency analysis and calculating the average of the differences between consecutive times of minimum lights. The q -search technique was used to estimate the initial values of mass ratios. The TESS light curve solutions indicated that the systems are detached eclipsing binaries. Unlike the other systems, a better fit was achieved by assuming a spotted area on the secondary component of CD-34 13220. We calculated the absolute parameters of the components of systems considering our analyses results by using `ABSPAREB` software (Liakos 2015) and list in Table 3. The masses of the primary components were estimated by using the stellar tracks for solar abundances of Bertelli et al. (2009) based on their $\log g$ and effective temperature. We conclude that the components of HD 295082 have very close mass and radius values while the secondary component of TYC 6527-2310-1 is more massive and luminous than the primary. The results implied that CD-34 13220 and TYC 6484-426-1 are typical detached binary systems.

The four systems were compared to 162 well-known detached binaries cataloged by Southworth (2015). In general, the locations of the components are in agreement with the other detached binary systems on the mass-radius plane and the Hertzsprung-Russell diagram (Fig. 6). However, it must be pointed out that the secondary component of CD-34 13220 is found to be slightly less massive according to its radius. The components of TYC 6484-426-1 almost overlap on the Hertzsprung-Russell diagram because of their similarity in temperature and luminosity. The location of the systems were also plotted with the six evolutionary tracks of Bressan et al. (2012) for masses from $0.9 M_{\odot}$ to $1.4 M_{\odot}$ in Fig. 7. The components of the systems seem to follow the evolution of the stars, having the initial masses of between 0.9 and $1.4 M_{\odot}$. The figure also

Table 3 Absolute parameters of the systems. TYC 6484 and TYC 6527 refer to TYC 6484-426-1 and TYC 6527-2310-1, respectively. The standard errors are given in parentheses for the last digits

Parameter	CD-34 13220	HD 295082	TYC 6484	TYC 6527
$M_1 (M_\odot)$	1.2	1.3	2.5	1.8
$M_2 (M_\odot)$	0.532(1)	1.301(1)	1.345(3)	2.151(4)
$R_1 (R_\odot)$	1.14(5)	2.17(3)	1.9(5)	2.0(1)
$R_2 (R_\odot)$	1.08(9)	2.74(3)	1.8(6)	2.90(8)
$L_1 (L_\odot)$	1.8(2)	6.4(5)	4(2)	4.8(7)
$L_2 (L_\odot)$	1.3(2)	9.1(8)	4(2)	9.4(9)
$a (R_\odot)$	5.736(4)	12.165(5)	24.83(1)	14.367(9)

primaries which led us to consider the possibility of enhanced stellar winds discussed by Tout & Eggleton (1988). The authors focused on mass inversion in RS CVn binaries and indicated that the secondary (originally less massive) component demonstrates tidally enhanced mass loss by the stellar wind. They also propose three different evolution scenarios based on Roche lobe overflow (RLOF) phase and period-mass ratio relation. Although the system Z Her used by authors in their model, shows some distinctive properties than our systems in terms of differences between radii and luminosities of the components, our derived mass ratios, and the mass values are agreed with the model star. According to their classification criteria based on final period and mass ratio, HD 295082 and TYC 6527-2310-1 are in the group of the systems whose RLOF stage begins at $q > 0.7$ and causes rapid mass transfer through common envelope evolution. We remark that the enhanced stellar wind mechanism is within the realm of possibility in describing the evolved status of secondary components. However, the hypothesis needs to be confirmed by detailed stellar models which reveal the initial orbital period and the masses of the systems.

We compared our targets to LAMOST EA-type eclipsing binaries whose properties are given by Qian et al. (2018). The distribution of the temperatures, orbital periods and $\log g$ values of LAMOST EA binaries are given in Fig. 8. We also drew box plots (Krzywinski & Altman 2014) of those three distributions (right panels of Fig. 8) to display the variation of the data and to examine its agreement with the parameters of our targets. The box plots indicate that the temperatures of the components of our systems are in good agreement with the same type of LAMOST stars. The orbital periods of CD-34 13220, HD 295082, and TYC 6527-2310-1 are in the interquartile range (*IQR*) as well. However, derived $\log g$ values deviate from the *IQRs*. The five-number summary of box plots is listed in Table 4 with the number of data and *IQRs* which were calculated by using the equation $IQR = Q_3 - Q_1$. Additionally, it is planned to inspect a relation among the given properties of LAMOST binaries (i.e. temperature, period, $\log g$, metallicity, and radial velocity) and compare to those of our targets. However, a correlation matrix (Fig. 9) constructed using a Python code based on data of 2906 LAMOST EA binaries implied that the parameters are weakly connected (the correlation coefficients are between -0.31 and 0.1) to end up with reliable results. As a consequence, our results suggest that the systems are expected to follow two different evolutionary courses as remarked by Qian et al. (2018); CD-34 13220 follow the evolutionary path from short-period EA system to less massive EW-type binary through AML. The other three long-period systems, on the other hand, are

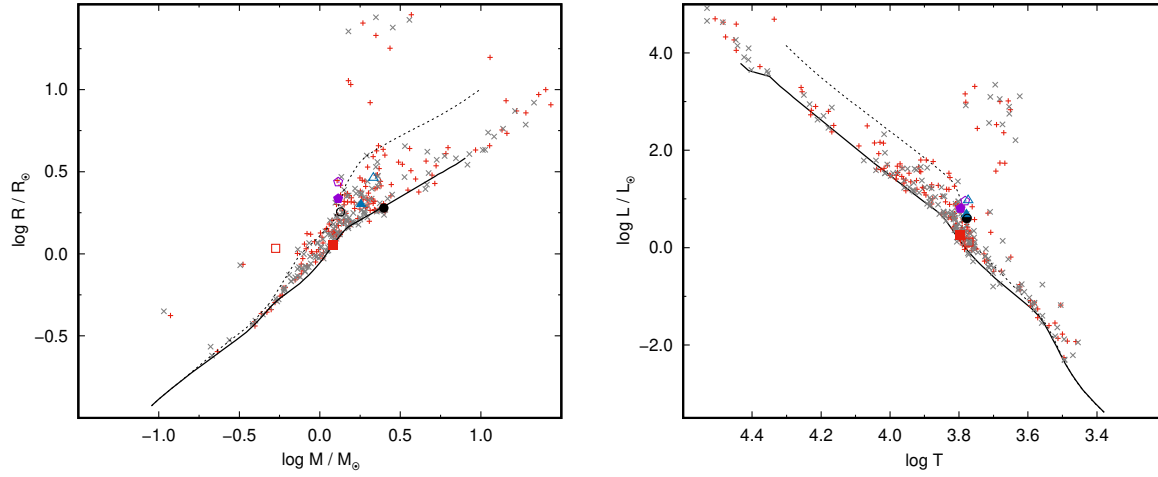


Fig. 6 Location of the components of the systems on the mass-radius plane (left) and the Hertzsprung-Russell diagram (right). Plus and crosses (pale colors; grey and tan in colored version) refer to the primary and secondary components of known detached systems given by Southworth (2015). Filled signs remark the primary components of the systems, where the open signs denote the secondaries. Squares (red), pentagons (purple), circles (black), and triangles (blue) refer to the components of CD-34 13220, HD 295082, TYC 6484-426-1, and TYC 6527-2310-1, respectively. The data for ZAMS (thick solid line) and TAMS (dashed line) with $Z=0.01$ and $Y=0.267$ abundance are taken from Bressan et al. (2012).

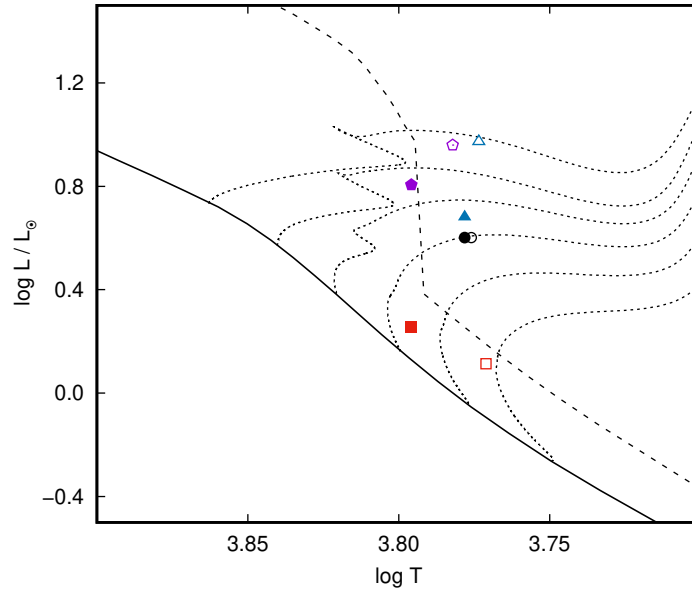


Fig. 7 Components of the systems on the Hertzsprung-Russell diagram with the evolutionary tracks for the stars with solar abundances and having the masses of $0.9 M_{\odot}$, $1.0 M_{\odot}$, $1.1 M_{\odot}$, $1.2 M_{\odot}$, $1.3 M_{\odot}$ and $1.4 M_{\odot}$ (dotted lines, from bottom to top). The other symbols are the same as those shown in Fig. 6. The evolutionary tracks, ZAMS (solid line) and TAMS (dashed line) data for $Z=0.01$ and $Y=0.267$ composition are adopted from Bressan et al. (2012).

Table 4 Summary of the box plots of LAMOST EA-type binaries. Temperature and period values are given in K and days, respectively

	Temperature	Period	$\log g$
Number of data	2956	2906	2956
Lower quartile ($Q1$)	5560	0.9063	4.03
Median ($Q2$)	6130	1.7671	4.15
Upper quartile ($Q3$)	6620	4.3571	4.28
Minimum	3970	0.2909	3.66
Maximum	8210	9.5240	4.65
IQR	1060	3.4508	0.25

We plausibly conclude that the systems are eclipsing detached binary systems. Advanced spectroscopic observations are needed for a more precise determination of the binary properties of the systems and to confirm the results presented in this study.

Acknowledgements This paper includes data collected by the TESS mission. Funding for the TESS mission is provided by the NASA's Science Mission Directorate. Some/all of the data presented in this paper were obtained from the Mikulski Archive for Space Telescopes (MAST). STScI is operated by the Association of Universities for Research in Astronomy, Inc., under NASA contract NAS5-26555. Support for MAST for non-HST data is provided by the NASA Office of Space Science via grant NNX13AC07G and by other grants and contracts. This research has made use of the NASA/IPAC Infrared Science Archive, which is operated by the Jet Propulsion Laboratory, California Institute of Technology, under contract with the National Aeronautics and Space Administration. This publication makes use of VOSA, developed under the Spanish Virtual Observatory project supported by the Spanish MINECO through grant AyA2017-84089. VOSA has been partially updated by using funding from the European Union's Horizon 2020 Research and Innovation Programme, under Grant Agreement n° 776403 (EXOPLANETS-A). This research has made use of NASA's Astrophysics Data System. This research has made use of the VizieR catalogue access tool, CDS, Strasbourg, France.

References

- Bayo, A., Rodrigo, C., Barrado Y Navascués, D., et al. 2008, *A&A*, 492, 277
- Bertelli, G., Nasi, E., Girardi, L., & Marigo, P. 2009, *A&A*, 508, 355
- Borucki, W. J., Koch, D., Basri, G., et al. 2010, *Science*, 327, 977
- Bressan, A., Marigo, P., Girardi, L., et al. 2012, *MNRAS*, 427, 127
- Cantat-Gaudin, T., Vallenari, A., Sordo, R., et al. 2018, *A&A*, 615, A49
- Claret, A. 2017, *A&A*, 600, A30
- Cruzalèbes, P., Petrov, R. G., Robbe-Dubois, S., et al. 2019, *MNRAS*, 490, 3158
- Cutri, R. M., Skrutskie, M. F., van Dyk, S., et al. 2003, *VizieR Online Data Catalog*, II/246
- Eggleton, P. P. 1983, *ApJ*, 268, 368
- Gaia Collaboration, Brown, A. G. A., Vallenari, A., et al. 2018, *A&A*, 616, A1

- Guinan, E. F. 1993, in *Astronomical Society of the Pacific Conference Series*, Vol. 38, *New Frontiers in Binary Star Research*, ed. K.-C. Leung & I.-S. Nha, 1
- Høg, E., Fabricius, C., Makarov, V. V., et al. 2000, *A&A*, 355, L27
- Kirk, B., Conroy, K., Prša, A., et al. 2016, *AJ*, 151, 68
- Kovaleva, D., Kaygorodov, P., Malkov, O., Debray, B., & Oblak, E. 2015, *Astronomy and Computing*, 11, 119
- Krzywinski, M., & Altman, N. 2014, *NATURE METHODS*, 11, 119
- Kurucz, R. L. 1979, *ApJS*, 40, 1
- Kwee, K. K., & van Woerden, H. 1956, *Bull. Astron. Inst. Netherlands*, 12, 327
- Lenz, P., & Breger, M. 2005, *Communications in Asteroseismology*, 146, 53
- Liakos, A. 2015, in *Astronomical Society of the Pacific Conference Series*, Vol. 496, *Living Together: Planets, Host Stars and Binaries*, ed. S. M. Rucinski, G. Torres, & M. Zejda, 286
- Lucy, L. B. 1967, *ZAp*, 65, 89
- Morrison, J. E., Röser, S., McLean, B., Bucciarelli, B., & Lasker, B. 2001, *AJ*, 121, 1752
- National Aeronautics and Space Administration. 1993, *Cape Photographic Durchmusterung*, 3
- Nesterov, V. V., Kuzmin, A. V., Ashimbaeva, N. T., et al. 1995, *A&AS*, 110, 367
- Niemela, V. 2001, in *Revista Mexicana de Astronomia y Astrofisica Conference Series*, Vol. 11, *Revista Mexicana de Astronomia y Astrofisica Conference Series*, 23
- Ochsenbein, F., Bauer, P., & Marcout, J. 2000, *A&AS*, 143, 23
- Pojmanski, G. 2002, *Acta Astronomica*, 52, 397
- Prša, A., & Zwitter, T. 2005, *ApJ*, 628, 426
- Qian, S. B., Zhang, J., He, J. J., et al. 2018, *ApJS*, 235, 5
- Qian, S.-B., Zhu, L.-Y., Liu, L., et al. 2020, *Research in Astronomy and Astrophysics*, 20, 163
- Qian, S.-B., Shi, X.-D., Zhu, L.-Y., et al. 2019, *Research in Astronomy and Astrophysics*, 19, 064
- Ricker, G. R., Winn, J. N., Vanderspek, R., et al. 2015, *Journal of Astronomical Telescopes, Instruments, and Systems*, 1, 014003
- Röser, S., Bastian, U., & Kuzmin, A. 1994, *A&AS*, 105, 301
- Ruciński, S. M. 1969, *Acta Astronomica*, 19, 245
- Ruiz-Dern, L., Babusiaux, C., Arenou, F., Turon, C., & Lallement, R. 2018, *A&A*, 609, A116
- Schofield, M., Chaplin, W. J., Huber, D., et al. 2019, *ApJS*, 241, 12
- Southworth, J. 2015, in *Astronomical Society of the Pacific Conference Series*, Vol. 496, *Living Together: Planets, Host Stars and Binaries*, ed. S. M. Rucinski, G. Torres, & M. Zejda, 164
- Stassun, K. G., Oelkers, R. J., Paegert, M., et al. 2019, *AJ*, 158, 138
- Tanenbaum, P., & Jenkins, J. M. 2018, *TESS Science Data Products Description Document*, EXP-TESS-ARC-ICD-0014 Rev D
- Thome, M. J. 1994, *VizieR Online Data Catalog*, I/114
- Tout, C. A., & Eggleton, P. P. 1988, *MNRAS*, 231, 823
- von Zeipel, H. 1924, *MNRAS*, 84, 665
- Wilson, R. E., & Devinney, E. J. 1971, *ApJ*, 166, 605

Zhao, G., Zhao, Y.-H., Chu, Y.-Q., Jing, Y.-P., & Deng, L.-C. 2012, *Research in Astronomy and Astrophysics*, 12, 723

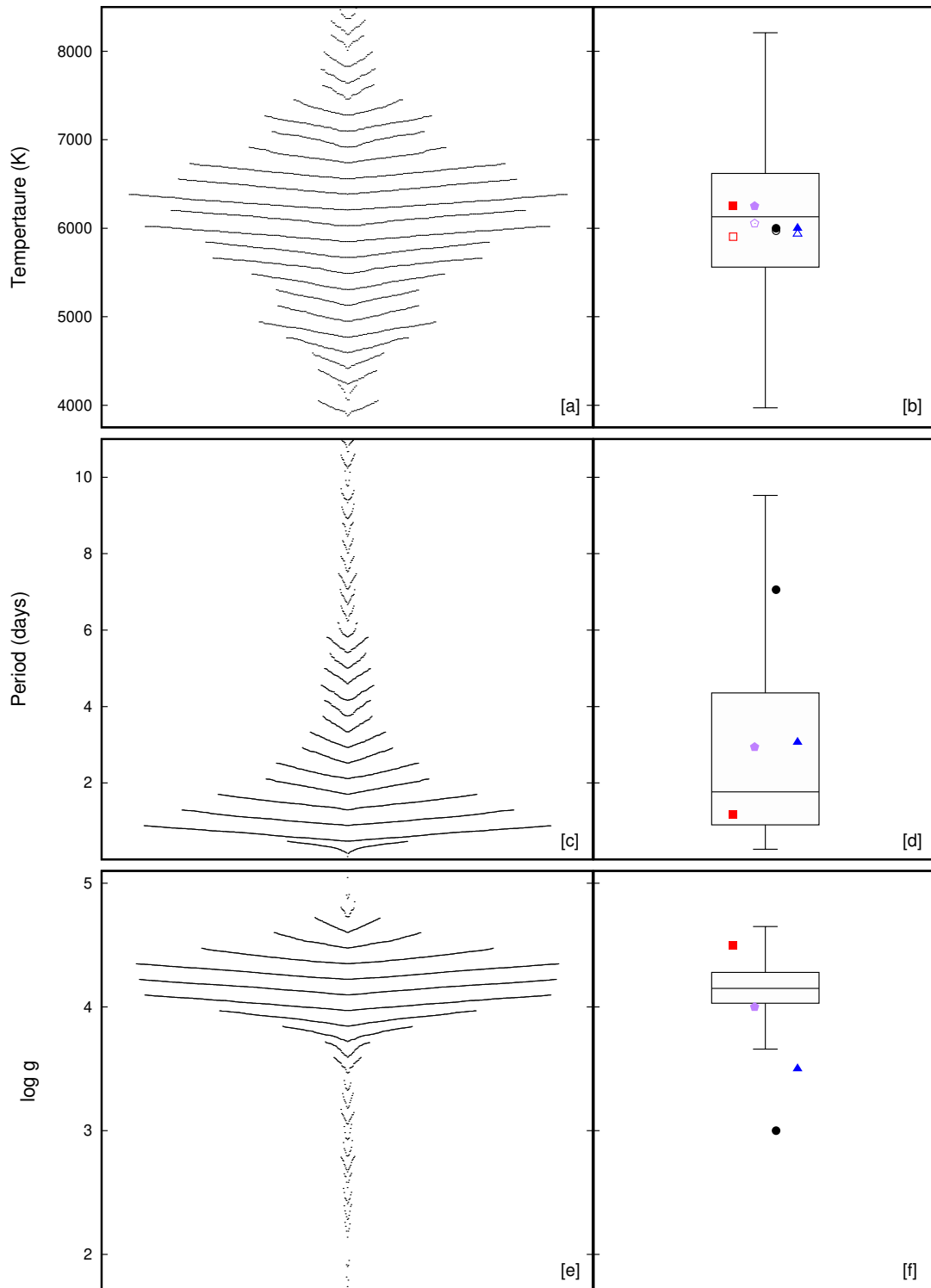


Fig. 8 Temperature (a), orbital period (c), and $\log g$ (e) distributions of EA-type LAMOST stars based on data from Qian et al. (2018) with their box plots (b, d, and e) where our targets are also flagged. Period values are plotted between 0 and 11 days (c) for the sake of clear visibility, although the box (d) calculated using the whole data interval. The symbols are the same as those shown in Fig. 6. See text for details.

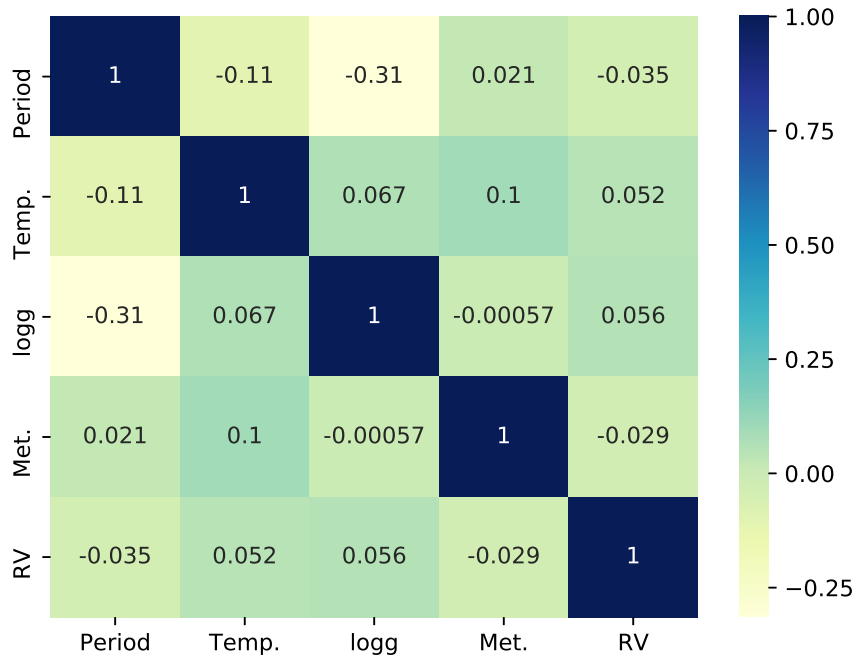


Fig. 9 Correlation matrix constructed based on parameter data of LAMOST EA stars given by Qian et al. (2018). Temp., Met., and RV stand for temperature, metallicity, and radial velocity.